Contributions to Geophysics and Geodesy Vol. 55/4, 2025 (539–556)

Impact of sea water intrusion on groundwater aquifers using geoelectrical techniques: A case study, the new port of Jarjob, El-Negila area, Marsa Matrouh, Egypt

Shimaa M. SALEM[1], Talaat Ali ABDELLATIF[1], Hosny M. Ezz EL DEEN[1], Islam N. EL-NEKHIELY[2], El-Arabi H. SHENDI[2,*]

[1] Desert Research Centre, Cairo, Egypt

[2] Faculty of Science, Suez Canal University, Ismailia, Egypt

Abstract: This research investigates the effect of seawater intrusion on groundwater quality in the western coastal zone of the Mediterranean Sea, Egypt, between Wadi Abu Emera and Abu-Hesha. The objective of this research is to study the effect of seawater intrusion on groundwater quality, using geoelectrical techniques including vertical electrical resistivity soundings (VES) and time-domain electromagnetic methods (TEM). Ten Schlumberger VES with a current electrode distance of as high as 600 m and twenty TEM soundings with a single loop of 200×200 metres were carried out during this study. Processing and interpretation of the field data concluded that the geoelectrical succession of the area consists of three layers, where the bottom layer is the water-bearing formation. Also, the resistivity values decrease with depth and towards the Mediterranean Sea because of the seawater intrusion. This intrusion occurs along a system of faults that act as conduits to bring seawater inland. It is recommended to avoid the locations of these faults while drilling wells unless these wells are used for the desalination process. These faults serve as conduits for seawater to migrate inland. In contrast, the southern portion of the survey area is suitable for well drilling, provided that careful measures are implemented to maintain the wells' safe yield.

Key words: Mediterranean Sea, vertical electrical sounding, transient electromagnetic sounding, water quality, coastal environment

1. Introduction

Seawater intrusion is a major threat to coastal areas, as it degrades groundwater aquifers and harms the region's development. This study investigates seawater intrusion in a 24 km^2 portion (approximately 5760 Faddan) of the

*corresponding author, e-mail: elarabi_shamais@science.suez.edu.eg

doi: 10.31577/congeo.2025.55.4.6

Mediterranean coastal zone, Egypt (Fig. 1). It has a stratigraphic sequence from the Middle Miocene to the Quaternary and features a seaward slope across coastal and piedmont plains and a southern tableland. It is very suitable for reclamation and tourism projects if water resources are available. The primary source of water for agricultural activities in this area is rainwater, but this source is insufficient. Accordingly, groundwater could emerge as the most practical complementary resource to supply the area with the necessary amount of water, but the intrusion of seawater is the common pollutant of the fresh groundwater in the study area. This phenomenon usually occurs in the coastal aquifers and can lead to a severe deterioration of the quality of fresh groundwater resources. Accordingly, a fresh saline water interface in the coastal regions needs an intensive geophysical study and monitoring for the assessment of the hydrological and hydrochemical parameters which are relevant to seawater intrusion (*Kumar et al., 2020; Kumar et al., 2022*). For this, geoelectrical exploration techniques are of great help to study the groundwater conditions, including seawater intrusion, and to locate suitable sites for drilling water wells. Additionally, the study area suffers from environmental issues due to progressive loss of freshwater and increases in water salinity. Several attempts were suggested to save water, such as rainwater harvesting, but the quantity was insufficient (*Ali et al., 2007*).

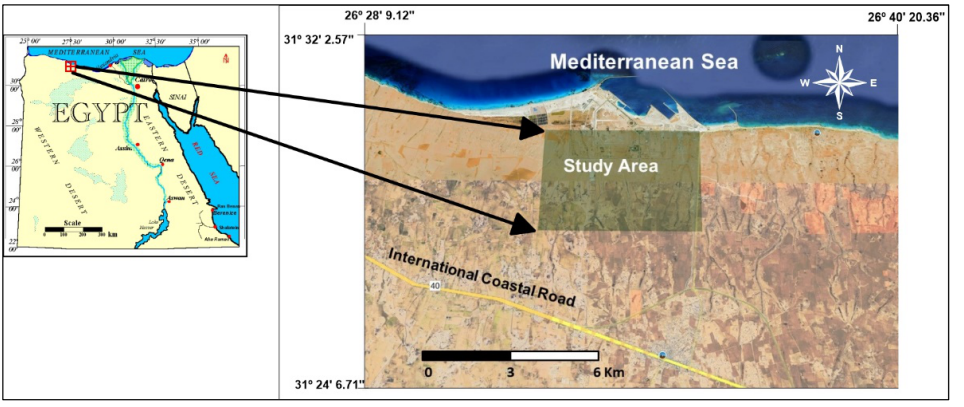

Fig. 1. Location map of the study area.

Twenty TEM soundings, in the form of a grid with a single loop of 200 × 200 metres, and ten Schlumberger VES, with a distance between the current

electrodes of as much as 600 m, were measured in the area. The objectives of these field measurements are to get more information about the suitable subsurface conditions for drilling water wells and to try to understand the seawater intrusion and its effect on the quality of the groundwater.

2. Geomorphological, geological, and hydrogeological settings

The study area is close to the coastal plain (Fig. 2), where different geomorphological and geological studies were carried out (*Shata, 1953, 1955 and 1971; Said, 1962; Abdallah, 1966a and 1966b; Sayed, 1967; Selim, 1969; Taha, 1973; Moussa, 1976; Raslan, 1995; Yousif and Bubenzer, 2013a and 2013b*). These studies concluded that a sub-arid climate characterises the region. In general, the average monthly temperature ranged from 14.4 to 26.8 °C and the average yearly rainfall ranged from 100 to 190 mm (*DRC internal report, 2010; Embaby et al., 2012*). Various geomorphological units were reported in the area (i.e., the coastal plain, the piedmont plain, the southern tableland, and the structural plateaus). The width of the coastal plain ranges from a few metres to several kilometres, and its altitude ranges from sea level to almost 100 metres. The piedmont plain consists of thick, fine calcareous soil with depressions, alluvial fans, and inland ridges. At

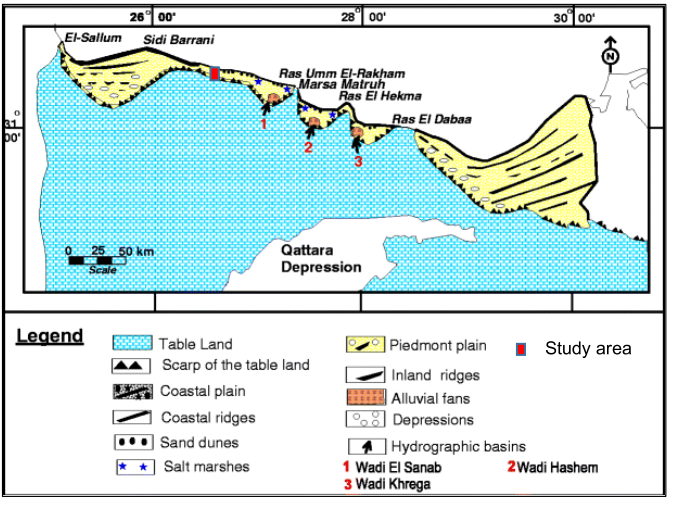

Fig. 2. Geomorphologic units of the northwestern coastal zone (after *Moussa, 1976*).

the same time, most of the tableland consists of cracked limestone, which is suitable to recharge the groundwater aquifers with rainwater. The structural plateau ranges in height from 100 to 160 metres, from south to north, along the piedmont plain.

Generally, the stratigraphic sequences of the northwestern coastal zone (Fig. 3) are mainly composed of sedimentary strata that range in age from Tertiary (Middle Miocene) to Quaternary (*Selim, 1969; Raslan, 1995*). The Middle Miocene and the Pliocene deposits are exposed in the area. The Middle Miocene deposits are represented by marine limestone with few clay intercalations, whereas the Pliocene deposits consist of pink, shallow marine, marly limestone. Folds and faults are common structures in the northwest coastal zone. In specific locations, fractures affect all the wadies which have different directions, such as NE–SW, E–W, and N–E. Pleistocene, Middle Miocene, and Holocene aquifers exist in the study area (*Yousif and Bubenzer, 2013a*).

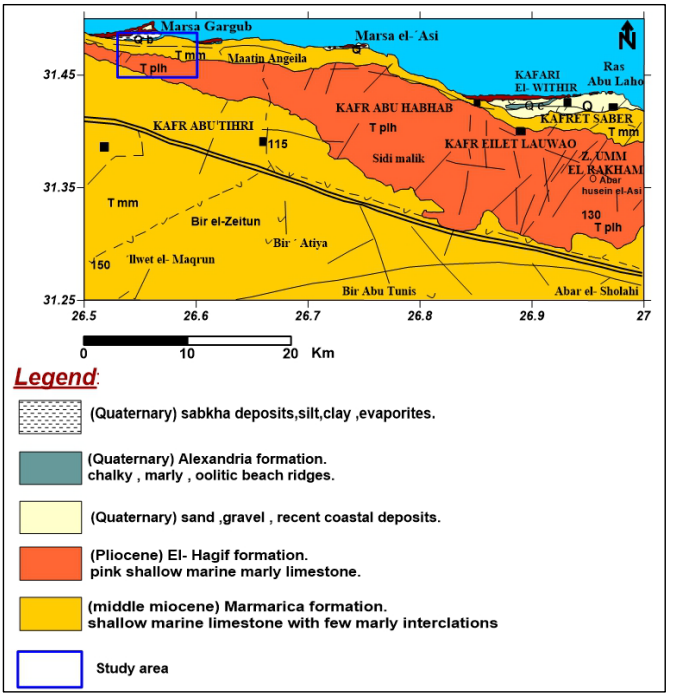

Fig. 3. Geologic map of the study area and surroundings (modified after *Conoco, 1986*).

3. Methodology

3.1. Transient Electromagnetic Method (TEM)

This method is a quick and economical way to get depths, ranging from a few metres to hundreds of metres. It can be used in various configurations and does not require direct electrical contact with the ground. It is an inductive method which works by passing a high current through a square loop placed on the ground. This current produces a time-varying primary magnetic field which penetrates the ground and causes eddy currents. These currents produce a secondary magnetic field. When the current is abruptly stopped, an electromagnetic induction occurs according to Faraday's law. The intensity of the eddy currents depends on the resistivity of the ground at a given depth and time (*Kaufman and Keller, 1983; Al-Garni and El-Kaliouby, 2011; Fitterman, 2014; El-Kaliouby and Abdalla, 2015; Bou-Rabee et al., 2025; Rajab et al., 2025*). Maxwell's equations describe electromagnetic field behaviour at any frequency, and for a medium that is polarisable and magnetisable, they can be expressed as:

$$\nabla\cdot\mathbf{D} = \boldsymbol{\rho}\,,$$
$$\nabla\cdot\mathbf{B} = 0\,,$$
$$\nabla\times\mathbf{E} = -\,\partial\mathbf{B}/\partial t\,,$$
$$\nabla\times\mathbf{H} = \boldsymbol{j} + \partial\mathbf{D}/\partial t\,,$$

where $\mathbf{E}$ is the electric field, $\mathbf{B}$ is magnetic induction, $\mathbf{H}$ is the magnetic field strength, $\mathbf{D}$ is electric displacement, $\boldsymbol{j}$ is the electric current density owing to free charges and $\boldsymbol{\rho}$ is the electric charge density owing to free charges. Curl ($\nabla\times$) and div ($\nabla\cdot$) are vector calculus expressions.

In this study, field TEM measurements were acquired by setting the time range of transient characteristics to 7 or 9 seconds. The induced current was set to 4A and the frequency of the filter was set to 50 Hz to improve the quality of the collected measurements. Twenty TEM soundings were acquired in the study area (Fig. 5) using a TEM-FAST 48HPC instrument with a loop size of 200×200 m. The measurement procedure involved repeatedly applying and stopping a transmitter current at a single location. During each cycle, a series of receiver output voltage values was recorded over a succession of time windows, with the timing dependent on the desired investigation depth. The data was automatically logged and stored

for operator review. By taking multiple repeat measurements, the repeatability of the field data can be checked, and all logged data can be processed to improve the signal-to-noise ratio. The acquired TEM data, in the form of apparent resistivities versus time, were processed and inverted using ZondTEM1D software.

3.2. Vertical Electrical Sounding (VES)

Electrical resistivity survey has been recognised as one of the most efficient techniques for the quantitative and qualitative assessment of groundwater resources. This analysis of surface electrical resistivity has often been used in aquifers to evaluate the extent of saline intrusion inland (*Choudhury et al., 2001; Mogren, 2015; Sherif et al., 2006; Kumar et al., 2021*). Earlier studies have also focused on the technique for tracking marine intrusion (*Bouderbala and Remini, 2014; Shammas and Jacks, 2007; Sung-Ho et al., 2007*). Subsurface resistivity is a useful parameter for estimating the extent of saline intrusion (*Satriani et al., 2012; Singh et al., 2021; El-Deen, 2005*). The large differences between the resistivity of saltwater and fresh water have been used in numerous investigations to determine saltwater intrusion in coastal areas (*Gurunadha Rao et al., 2011; Khublaryan et al., 2008; Kouzana et al., 2010; Alfaifi et al., 2019*). The most commonly used methods for measuring earth resistivity are those in which current is driven through the ground using a galvanic contact. Current is driven through one pair of electrodes (**A** & **B**) and the potential established in the earth by this current is measured with the second pair of electrodes (**M** & **N**) connected to a sensitive voltmeter (Fig. 4). It is then possible to determine an effective or apparent resistivity of the subsurface.

In studying the variation of resistivity with depth, as in the case of a layered medium, the spacing between the various electrodes are generally

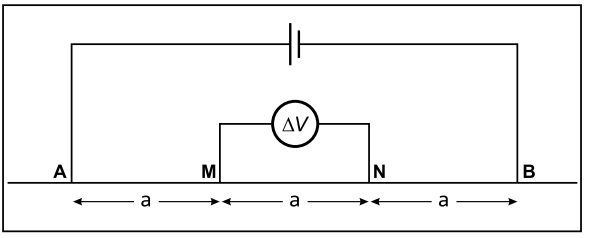

Fig. 4. Electrode layout during vertical electrical sounding.

increased with larger spacing, the effect of the material at depth on the measurements becomes more pronounced. This type of measurements is called a vertical sounding or electrical coring. The following equation can calculate the apparent resistivity of the subsurface materials:

$$\rho_a = \frac{\Delta V}{I}\left(\frac{2\pi}{\frac{1}{\mathrm{AM}} - \frac{1}{\mathrm{BM}} - \frac{1}{\mathrm{AN}} + \frac{1}{\mathrm{BN}}}\right).$$

Ten soundings were measured in this study, along profiles perpendicular to the sea coast (Fig. 5). Some of these soundings were measured close to water wells to estimate the resistivity spectrum of the area and to facilitate the interpretation of the other soundings. Additionally, other soundings were measured near TEM soundings for the purpose of correlation and confirmation of the results. Schlumberger array was used where the current electrodes distance reaches up to 600 m. The device that was used to collect the field data is a SYSCAL JUNIOR resistivity meter.

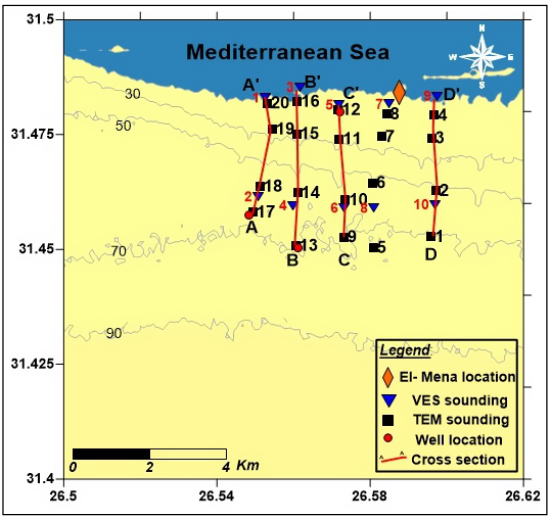

Fig. 5. Location map of TEM and VES soundings, water wells and cross-sections.

4. Results

The field data of the Transient Electromagnetic (TEM) soundings were filtered, smoothed, and converted to apparent resistivities versus time (ρ and t) prior to the inversion process. Also, the VES curves represent the vari-

ation of resistivity with depth. Figure 6 shows TEM and VES curves near a water well, illustrating the variation in resistivity with depth. There is a great similarity between the two curves. They both indicate a decrease in the value of electrical resistivity at depth, as it reaches its lowest value at great depth. This may confirm the idea of seawater intrusion. Table 1 contains the obtained VES and TEM results in the study area.

Table 1. Geoelectrical data of the study area.

Section	Trend and Length	TEM no., VES no. and wells	Geoelectrical layers, resistivity and thickness					
			Surface layer "A"	Layer "B"		Layer "C"		
				Zone "B1"	Zone "B2"	Zone "C1"	Zone "C2"	Zone "C3"
A–A′	N–S 4.4 km	TEM no. 13, 14,15,16 & VES 1,2 & Well 1	43.8–195 Ω.m 1–3 m	6.5–121.5 Ω.m 2–9 m	9.9–95.13 Ω.m 15–61 m	7.25–16.23 Ω.m 3–5 m	1.81–5.25 Ω.m 21 m	0.29–2.48 Ω.m —
B–B′	N–S 3.8 km	TEM no. 9, 10,11,12 & VES 3,4 & Well 2	25.3–162.2 Ω.m 1–2 m	2.1–25.9 Ω.m 4–5 m	12.1–46.27 Ω.m 3–63 m	9–16.14 Ω.m 13–40 m	1.47–3.34 Ω.m 22 m	0.6–0.73 Ω.m —
C–C′	NW–SE 4 km	TEM no. 9, 10,11,12 & VES 5,6 & Well 3	34.1–81.5 Ω.m 2–4 m	4.7–41 Ω.m 2–7 m	10.9–355 Ω.m 5–60 m	6.27–13.7 Ω.m 17–43 m	1.43–4.28 Ω.m 11 m	0.36–4.2 Ω.m —
D–D′	N–S 3.4 km	TEM no. 1,2, 3,4 & VES 9,10	75–84.5 Ω.m 2–3 m	13.2–26.6 Ω.m 7–16 m	24.01–72.2 Ω.m 38–57 m	6.2–10.8 Ω.m 16–30 m	1–3.6 Ω.m 29 m	0.6–0.68 Ω.m —

Note: the fitting error percentage in the models for all VES and TEM soundings is 5ess than 5%.

5. Discussion

The qualitative interpretation of the TEM and VES data involves comparing the relative changes in the apparent resistivity and thickness of the different layers. It gives information about the number of the geoelectrical layers, their continuity throughout the area or in a specific direction, and their degree of homogeneity or heterogeneity. It also gives information about the curve types, their areal distribution, and the lateral and vertical variations of resistivity values all over the study area. On the other hand, the quantitative interpretation reflects the number of subsurface geoelectrical layers, their thicknesses, and their apparent resistivities. Interpretation of both TEM and VES soundings area was carried out by using several software such as ATO (*Zohdy, 1989*), RESIST (*Vander Velpen, 1988*), RESIX-PLUS (*Interpex Ltd., 1996*), IPI2Win (*IPI2Win, 2003*), ZondTEM1D (*Kaminsky, 2001*) and IX1D (*Interpex Ltd., 2008*).

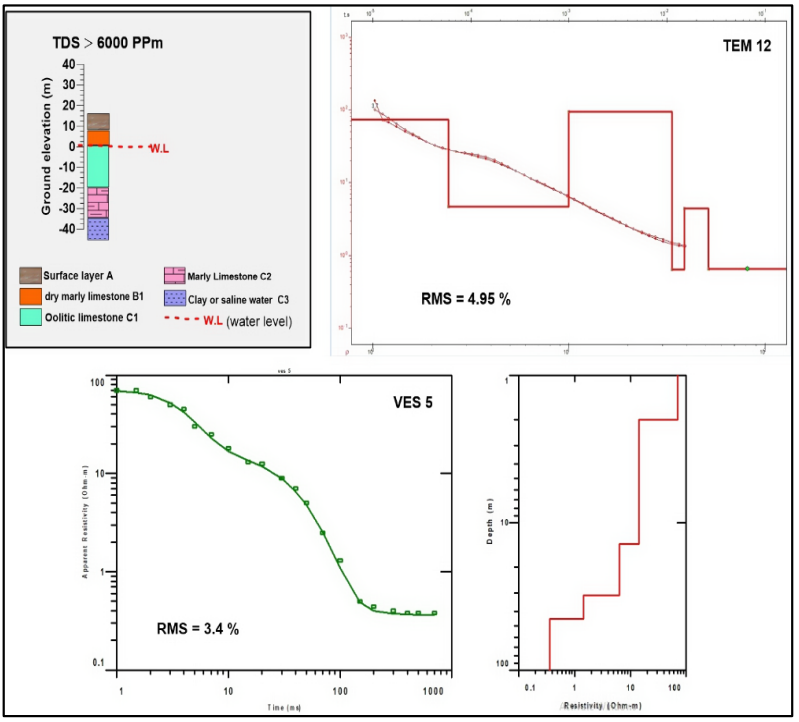

Fig. 6. Example of VES and TEM sounding close to water well in the study area.

The VES curves of the study area are of the QQQ and HKQ types (Fig. 6, as an example). In general, the resistivities of the first and second cycles of the VES curves reflect the heterogeneity of the surface and near-surface sediments, which are composed of dry gravel and sand. The third cycle, on the other hand, reflects the homogeneity of the subsurface layers. However, all the VES curves are terminated by Q-type, indicating that the resistivity values decrease seriously with depth, which can be interpreted as seawater intrusion. The quantitative Interpretation of the VES curves, in the light of the available water wells data, indicates a subsurface geoelectrical section consisting of three layers. The near-surface two layers are composed of dry sediments, whereas the bottom layer is the water-bearing formation of Miocene deposits. A detailed description of these layers indicates that the surface layer A is composed of dry sand, gravel, and clay of Recent age. This layer has resistivity values ranging from 25 to 195 Ohm·m and a thickness

that varies from 1 to 4 m (Fig. 7 and Table 1). This variation in resistivity is mainly due to lithological changes. This map also shows low resistivity zones running both in the NE–SW and NW–SE directions. These zones may represent buried drainage lines of shallow depths, which can be considered during the drilling program of shallow water wells.

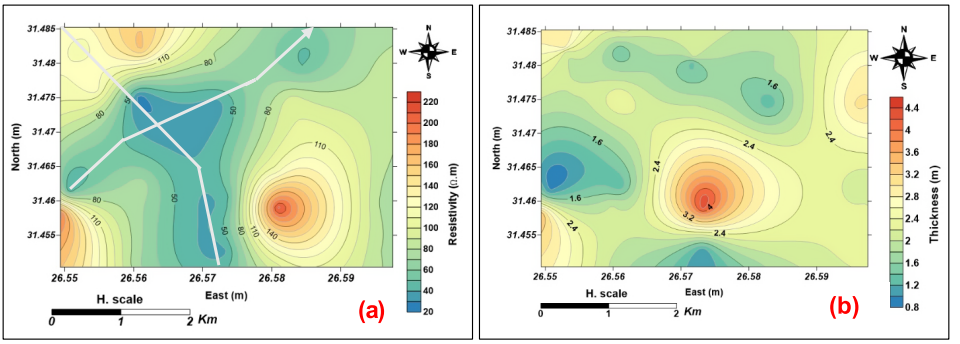

Fig. 7. Iso-resistivity map (a) and thickness map (b) of the surface layer A.

Layer B can be subdivided into two zones B1 and B2 (Table 1 and Figs. 12 and 13). Depending on the available geological information, zone B1 consists of marly limestone with a resistivity ranging from 2 to 121 Ω·m and a thickness varying from 2 to 16 m, while zone B2 consists of dry limestone with clay intercalations. Its resistivity ranges from 10 to 355 Ω·m and its thickness varies from 3 to 63 m (Fig. 8). In general, the resistivity and thickness values of layer B decrease towards the Mediterranean Sea and vice versa. This map also shows low resistivity zones running both in the NW–SE and NE–SW directions. These zones may represent buried drainage lines passing through faults and managing the movement of seawater inland. The locations of these faults should be avoided during the drilling of water wells unless these wells are drilling for the desalination process.

Layer C represents the saturated water-bearing formation, which can be classified into three zones C1, C2, and C3 (Table 1 and Figs. 12 and 13) according to their resistivity values. The resistivity values of this layer decrease seriously towards the Mediterranean Sea with some parallel zones extending inland in the NW–SE direction (Fig. 9). It is believed that these zones represent fault zones which may act as conduits for seawater intrusion. These zones should be avoided while drilling water wells unless these wells

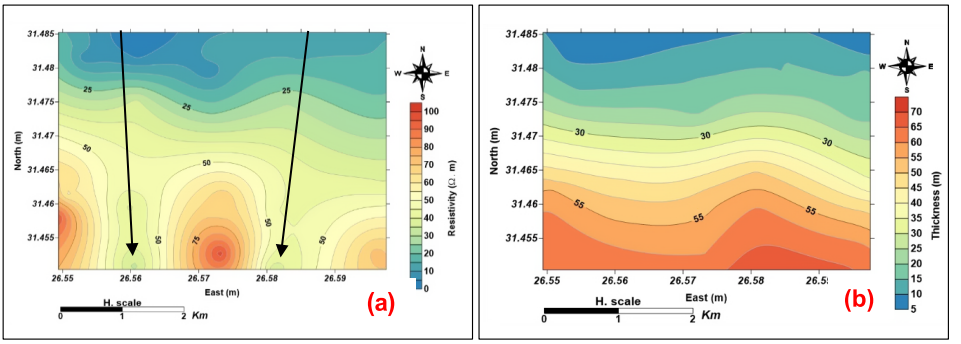

Fig. 8. Iso-resistivity map (a) and thickness map (b) of the layer B.

are drilled for desalination operations. In this case, the fault zones are considered the best sites for drilling wells because they will facilitate the passage of seawater towards these wells. Depending on the water wells' information, zone C1 consists of oolitic limestone and is saturated with brackish water. Its resistivity ranges from 6 to 16 Ω·m (Table 1) and its thickness varies from 3 to 43 m with a general increase in the south direction. Zone C2 consists of marly limestone and saturated with salt water. Its resistivity ranges from 1 to 5 Ω·m and its thickness ranges from 11 to 29 m (Table 1), in comparison, zone C3 consists of sandy clay to clay and saturated with very high salt water, which may be due to sea water intrusion. Its resistivity ranges from 0.29 to 4.2 Ω·m (Fig. 9a and Table 1). The depth to the water level in this layer ranges from 17 to 67 m, as recorded from the wells and interpreted from the geoelectrical study (Fig. 9b).

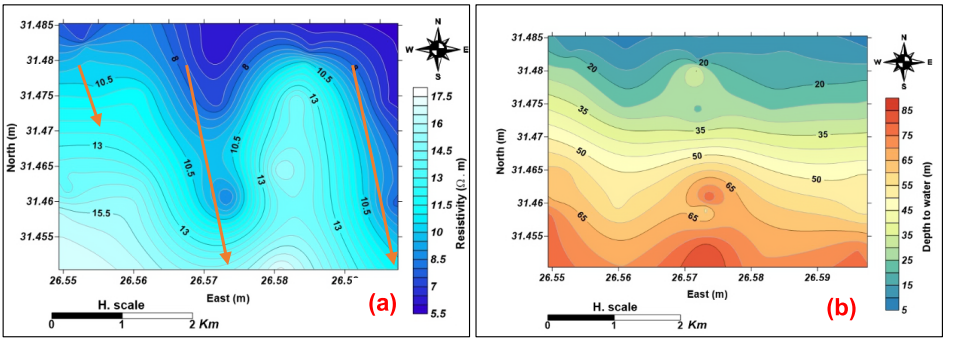

Fig. 9. Iso-resistivity map (a) and depth map (b) of layer C.

Sometimes, preparation of apparent resistivity sections (pseudo-sections) can contribute valuable information about the seawater intrusion. These sections are constructed by plotting the apparent resistivity values along vertical lines, beneath the sounding locations and these values are then contoured. Two pseudo-sections are constructed in the study area, one parallel and close to the sea coast (Fig. 10) and the other at a distance of about 2.5 km (Fig. 11). Figure 10 shows that the seawater intrusion occurs at shallow depth, where the resistivity values are extremely low. However, relatively high resistivity values are observed around VES numbers 1, 3, and 5, which can be attributed to hard rocks or dry soils. On the other hand, the pseudo-section in Fig. 11 shows that the seawater intrusion occurs at relatively deep depth, in comparison to the section which is close to the sea coast. Also, very low resistivity values around VES numbers 2 & 4 appear at shallow depth, which can be interpreted due to the occurrence of clay rich sediments. However, the results of the two sections should be considered while drilling wells to avoid the negative impact of the saltwater.

Moreover, four 2-D geoelectrical sections have been constructed in the area (i.e., A–A′, B–B′, C–C′, and D–D′) depending on the results of the TEM and VES measurements, in light of the subsurface geological information. These sections run from north to south to show the seawater intrusion. The seawater intrusion appears in the four sections as the resistivity values are seriously decreasing with depth (Figs. 12 and 13). The water salinity of well no. 3 confirms this conclusion, where its T.D.S. value reaches as high as 6000 ppm. This value decreases southwards to approximately 3000 ppm at wells numbers 1 & 2 (Fig. 12). Accordingly, precautions should be taken during the drilling of water wells close to the sea coast.

6. Conclusion

Geophysical studies have been conducted in the study area, located near the coast of the Mediterranean Sea, at the new port of Jarjob, El-Negila, Egypt. The main target of these studies is to evaluate the groundwater aquifer and the possibility of seawater intrusion. Ten VES, by Schlumberger array with a current electrode distance of as much as 600 m, and twenty TEM soundings, with a single loop of 200×200 m, have been measured. Processing and interpretation of the field data concluded that the subsurface geoelectrical

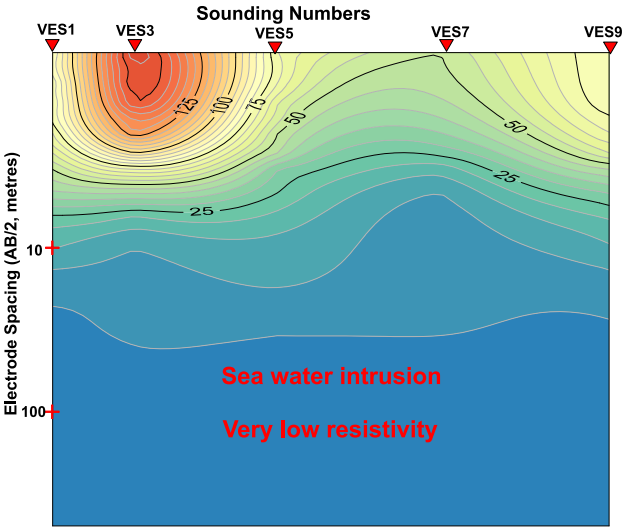

Fig. 10. Pseudo-section close to the sea coast passing through VES numbers $1, 3, 5, 7, 9$.

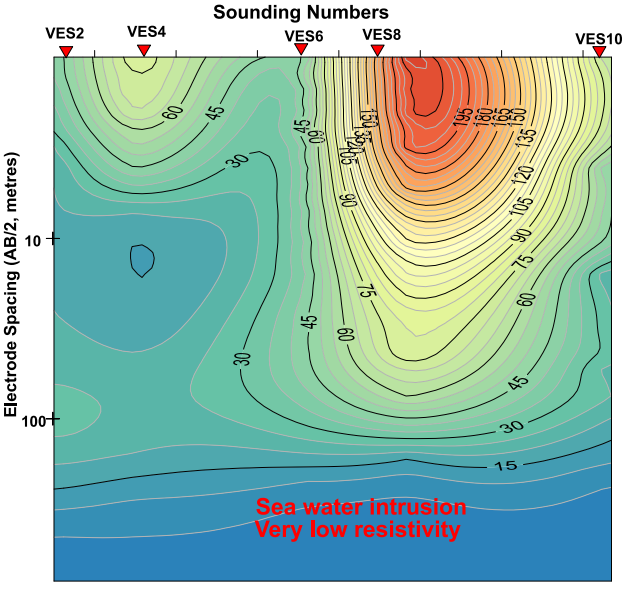

Fig. 11. Pseudo-section at the south of the study area between VES numbers $2, 4, 6, 8, 10$.

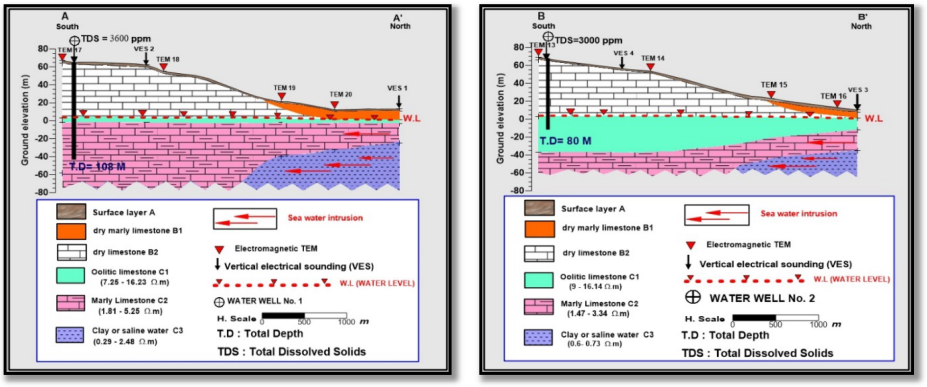

Fig. 12. Geoelectrical sections A–A′ and B–B′.

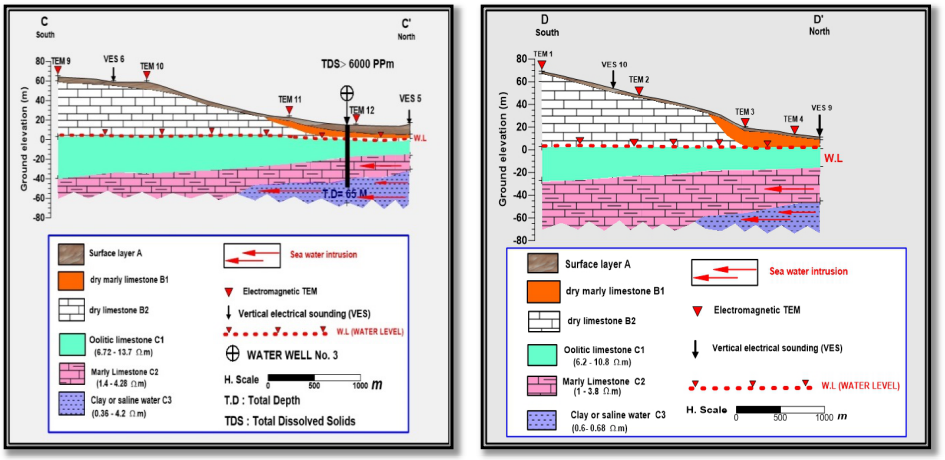

Fig. 13. Geoelectrical sections C–C′ and D–D′.

section of the area consists of three geoelectrical layers. The upper two layers are composed of dry gravel, sand, and clay deposits. The bottom layer is the water-bearing and consists of fractured limestone. This layer has a suitable saturated thickness reaching up to 25 metres, and its resistivity decreases with depth. Accordingly, precautions should be considered when drilling wells to consume the water of this layer to avoid the adverse effect of the deep salt water. The salinity of the water of this layer increases towards the Mediterranean Sea (i.e., 6000 ppm), which may confirm the effect of

seawater intrusion. This intrusion occurs along a system of faults, which facilitates the movement of seawater inland. It is recommended to avoid these faults while drilling wells unless they are drilled for the desalination process. However, the southern part of the area is suitable for drilling wells as the water salinity decreases to as low as 3000 ppm.

References

Abdallah A. M., 1966a: Geology of some gypsum deposits in the northwestern desert of Egypt. Geol. Surv. Egypt, Paper No. 41, 1–11 p.

Abdallah A. M., 1966b: Stratigraphy and structure of a portion in the northwestern desert of Egypt. Geol. Surv. Egypt, Paper No. 45, 1–19 p.

Ali A., Oweis T., Rashid M., El Naggar S., Aal A. A., 2007: Water harvesting options in the dry lands at different spatial scales. Land Use Water Resour. Res., **7**, 1–13, doi: 10.22004/ag.econ.48065.

Alfaifi H., Kahal A., Albassam A., Ibrahim E., Abdelrahman K., Zaidi F., Alhumidan S., 2019: Integrated geophysical and hydrochemical investigations for seawater intrusion: a case study in southwestern Saudi Arabia. Arab. J. Geosci., **12**, 12, 372, doi: 10.1007/s12517-019-4540-8.

Al-Garni M. A., El-Kaliouby H. M., 2011: Delineation of saline groundwater and seawater intrusion zones using transient electromagnetic (TEM) method, Wadi Thuwal area, Saudi. Arabia. Arab. J. Geosci. **4**, 3-4, 655–668, doi: 10.1007/s12517-009-0094-5.

Bou-Rabee F., Yogeshwar P., Burberg S., Tezkan B., Duane M., Ibraheem I. M., 2025: Imaging of groundwater salinity and seawater intrusion in Subiya peninsula, Northern Kuwait, using transient electromagnetics. Water, **17**, 5, 652, doi: 10.3390/w17050652.

Bouderbala A., Remini B., 2014: Geophysical approach for assessment of seawater intrusion in the coastal aquifer of Wadi Nador (Tipaza, Algeria). Acta Geophys., **62**, 6, 1352–1372, doi: 10.2478/s11600-014-0220-y.

Choudhury K., Saha D. K., Chakraborty P., 2001: Geophysical study for saline water intrusion in a coastal alluvial terrain. J. Appl. Geophys., **46**, 3, 189–200, doi: 10.1016/S0926-9851(01)00038-6.

CONOCO, 1986: Geological map of Egypt, scale 1:500,000. EGPC, sheet No. NH 35 NW (Salum).

DRC (Desert Research Center) internal report, 2010: Integrated Agriculture Development of Northwestern coastal wadies. Annual report. Desert Research Center publications, Cairo, Egypt.

El-Deen H. M. E., 2005: Geoelectrical study on the groundwater occurrences in Delta Wadi Hodein, Shalateen area, Red Sea, southeast of Egypt. Tethys Geological Society.

El-Kaliouby H., Abdalla O., 2015: Application of time-domain electromagnetic method in mapping saltwater intrusion of a coastal alluvial aquifer, North Oman. J. Appl. Geophys., **115**, 59–64, doi: 10.1016/j.jappgeo.2015.02.003.

Embaby A. A. A., Shanab S. E. A., 2012: Geochemistry of quaternary aquifer groundwater in Burg El Arab area and its suitability for irrigation. J. Am. Sci., **8**, 12, 1366–1377, doi: 10.7537/marsjas081212.184.

Fitterman D. V., 2014: Mapping saltwater intrusion in the Biscayne aquifer, Miami-Dade County, Florida, using transient electromagnetic sounding. J. Environ. Eng. Geophys., **19**, 1, 33–43, doi: 10.2113/JEEG19.1.33.

Gurunadha Rao V. V. S., Tamma Rao G., Surinaidu L., Rajesh R., Mahesh J., 2011: Geophysical and geochemical approach for seawater intrusion assessment in the Godavari Delta basin, A.P., India. Water Air Soil Pollut., **217**, 1-4, 503–514, doi: 10.1007/s11270-010-0604-9.

Interpex Ltd., 1996: RESIX-PLUS. Resistivity data interpretation software, v. 2.39. Golden, Colorado, USA.

Interpex Ltd., 2008: IX1Dv2. Resistivity data interpretation software, v. 1.0., Golden, Colorado, USA.

IPI2Win, 2003: Resistivity sounding interpretation software, ver. 3.0.1.a. Moscow State Univ., Moscow, Russia, available online: http://geophys01.geol.msu.ru/ipi2win.htm.

Kaminsky A., 2001: ZondTEM1D (software). Zond Software Corporation, available online: http://zond-geo.com/english/zond-software/electromagnetic-sounding/zondtem1d/.

Kaufmann A. A., Keller G. V., 1983: Frequency and Transient Soundings (Methods in Geochemistry and Geophysics). Elsevier Publ. Co., Vol. 16, Amsterdam, 685 p.

Khublaryan M. G., Frolov A. P., Yushmanov I. O., 2008: Seawater intrusion into coastal aquifers. Water Resour., **35**, 3, 274–286, doi: 10.1134/S0097807808030032.

Kouzana L., Benassi R., Ben Mammou A., Sfar Felfoul M., 2010: Geophysical and hydrochemical study of the seawater intrusion in Mediterranean semiarid zones. Case of the Korba coastal aquifer (Cap-Bon, Tunisia). J. Afr. Earth Sci., **58**, 2, 242–254, doi: 10.1016/j.jafrearsci.2010.03.005.

Kumar P., Tiwari P., Biswas A. Acharya T., 2020: Geophysical and hydrogeological investigation for the saline water invasion in the coastal aquifers of West Bengal, India: A critical insight in the coastal saline clay-sand sediment system. Environ. Monit. Assess., **192**, 9, 562, doi: 10.1007/s10661-020-08520-x.

Kumar P., Tiwari P., Singh A., Biswas A., Acharya T., 2021: Electrical Resistivity and Induced Polarization signatures to delineate the near-surface aquifers contaminated with seawater invasion in Digha, West-Bengal, India. Catena, **207**, 105596, doi: 10.1016/j.catena.2021.105596.

Kumar P., Tiwari P., Biswas A., Acharya T., 2022: Geophysical investigation for seawater intrusion in the high-quality coastal aquifers of India: A review. Environ. Sci. Pollut. Res., **30**, 4, 9127–9163, doi: 10.1007/s11356-022-24233-9.

Mogren S., 2015: Saltwater intrusion in Jizan coastal zone, southwest Saudi Arabia, inferred from geoelectric resistivity survey. Int. J. Geosci., **6**, 3, 286–297, doi: 10.4236/ijg.2015.63022.

Moussa B. M., 1976: Geomorphology and subsurface geology of the area between El Alameein and Qattara depression, Northern Western Desert, Egypt. Unpub. M.Sc. Thesis, Ain shams Univ., Cairo, Egypt.

Rajab J. A., Yogeshwar P., Tezkan B., Al-Halbouni D., 2025: Transient electromagnetic imaging of saltwater intrusion at the shrinking Dead Sea. Sci. Rep., **15**, 30250, doi: 10.1038/s41598-025-15189-0.

Raslan S. M., 1995: Geomorphological and hydrological studies on some localities along the Northwestern Coast of Egypt. M.Sc. Thesis, Faculty of Science, Menoufia University.

Said R., 1962: The geology of Egypt. Elsevier Publ. Co., Amsterdam, 377 p.

Satriani A., Loperte A., Imbrenda V., Lapenna V., 2012: Geoelectrical surveys for characterization of the coastal saltwater intrusion in Metapontum Forest Reserve (Southern Italy). Int. J. Geophys., **2012**, 1, 238478, 8 p., doi: 10.1155/2012/238478.

Sayed M. A. A., 1967: Geophysical study on the groundwater resources of Ras El-Hekma area, northwestern littoral zone of Egypt. M.Sc. Thesis, Faculty of Science, Cairo University, 129 p.

Selim A. A., 1969: Geology of El Salum area western Mediterranean coastal zone, U.A.R. Ph.D. Thesis, Faculty of Science, Alexandria Univ., 5–19.

Shammas M. I., Jacks G., 2007: Seawater intrusion in the Salalah plain aquifer, Oman. J. Environ. Hydrol., **15**, 19.

Shata A. A., 1953: New light on the structural development of the Western desert of Egypt. Bull. Desert Res. Inst., **3**, 1, 101–106.

Shata A. A., 1955: An introductory note on the geology of the northern portion of the Western Desert of Egypt. Bull. Desert Res. Inst., **5**, 2, 96–106.

Shata A. A., 1971: The geomorphology, pedology and hydrogeology of the Mediterranean coastal desert of U.A.R. In: Gray C. (Ed.): Proc. Symposium on the geology of Libya, Tripoli, Libya, pp. 431–446.

Sherif M., El Mahmoudi A., Garamoon H., Kacimov A., Akram S., Ebraheem A., Shetty A., 2006: Geoelectrical and hydrogeochemical studies for delineating seawater intrusion in the outlet of Wadi Ham, UAE. Environ. Geol., **49**, 4, 536–551, doi: 10.1007/s00254-005-0081-4.

Singh S., Gautam P. K., Kumar P., Biswas A., Sarkar T., 2021: Delineating the characteristics of saline water intrusion in the coastal aquifers of Tamil Nadu, India by analysing the Dar-Zarrouk parameters. Contrib. Geophys. Geod., **51**, 2, 141–163, doi: 10.31577/congeo.2021.51.2.3.

Sung-Ho S., Jin-Yong L. Namsik P., 2007: Use of vertical electrical soundings to delineate seawater intrusion in a coastal area of Byunsan, Korea. Environ. Geol., **52**, 6, 1207–1219, doi: 10.1007/s00254-006-0559-8.

Taha H. A., 1973: Geology of the water supplies of Matruh-Barrani area, northwestern Mediterranean coastal zone, Egypt. Ph.D. Thesis, Faculty of Science, Alexandria Univ., p. 5–19.

Vander Velpen B. P. A., 1988: Computer program "Resist", ver. 1.0. M.Sc. Thesis, ITC, Delft, Netherlands.

Yousif M., Bubenzer O., 2013a: An integrated approach for groundwater assessment at the Northwestern Coast of Egypt (Ras El Hekma area): Case study. Environ. Earth Sci., **69**, 7, 2227–2246, doi: 10.1007/s12665-012-2052-x.

Yousif M., Bubenzer O., 2013b: Integrated remote sensing and GIS for surface water development. Case study: Ras El Hekma area, northwestern coast of Egypt. Arab. J. Geosci., **6**, 4, 1295–1306, doi: 10.1007/s12517-011-0433-1.

Zohdy A. A. R., 1989: A new method for the automatic interpretation of Schlumberger and Wenner sounding curves. Geophysics, **54**, 2, 245–253, doi: 10.1190/1.1442648.